Journal of Hazardous Materials 193 (2011) 120–127

Contents lists available at ScienceDirect

Journal of Hazardous Materials

journal homepage: www.elsevier.com/locate/jhazmat

Improved photocatalytic degradation rates of phenol achieved using novel porous ZrO_2-doped TiO_2 nanoparticulate powders

Colm McManamon[a,*], Justin D. Holmes[a,b], Michael A. Morris[a,b]

[a] Department of Chemistry, Supercritical Fluid Centre and Materials Section, University College Cork, Cork, Ireland
[b] Environmental Research Institute (ERI), Lee Road, Cork, Ireland

ARTICLE INFO

Article history:
Received 13 May 2011
Received in revised form 6 July 2011
Accepted 8 July 2011
Available online 19 July 2011

Keywords:
Photocatalysis
TiO_2
Nanoparticles
Phenol degradation

ABSTRACT

This paper studies the photocatalytic degradation of phenol using zirconia-doped TiO_2 nanoparticles. ZrO_2 was chosen due to its promising results during preliminary studies. Particles smaller than 10 nm were synthesised and doped with quantities of ZrO_2 ranging from 0.5 to 4% (molar metal content). Particles were calcined at different temperatures to alter the TiO_2 structure, from anatase to rutile, in order to provide an ideal ratio of the two phases. Powder X-ray diffraction (PXRD) analysis was used to examine the transformation between anatase and rutile. Degradation of phenol was carried out using a 40 W UV bulb at 365 nm and results were measured by UV–vis spectrometry. TEM images were obtained and show the particles exhibit a highly ordered structure. TiO_2 doped with 1% ZrO_2 (molar metal content) calcined at 700 °C proved to be the most efficient catalyst. This is due to an ideal anatase:rutlie ratio of 80:20, a large surface area and the existence of stable electron–hole pairs. ZrO_2 doping above the optimum loading acted as an electron–hole recombination centre for electron–hole pairs and reduced photocatalytic degradation. Synthesised photocatalysts compared favourably to the commercially available photocatalyst P25. The materials also demonstrated the ability to be recycled with similar results to those achieved on fresh material after 5 uses.

1. Introduction

Since Fujishima and Honda (1972) discovered photoelectrolysis of water, TiO_2 has been used to decompose pollutants without the application of an external voltage [1]. Single crystal n-type TiO_2 (rutile) semiconductor electrodes with a positive valance band edge were shown to oxidize water to oxygen [2]. This discovery led Frank and Bard, in 1977, to use TiO_2 for the oxidation of cyanide in water [3]. Since then, TiO_2 has being used in a wide variety of applications such as a photocatalyst in solar cells for the production of hydrogen and electric energy, in electronic devices and in optical coatings [2]. Much recent attention has been focused on the use of TiO_2 for environmental remediation. Commercial products such as self-cleaning glass, air purification filters and disinfectant tiles show a market for the environmental applications of photocatalysis [4]. The reasons for so much attention being given to TiO_2 is that it is an extremely stable material and relatively inexpensive, it is also thought to be environmentally friendly, non-toxic and poses little threat to humans [2]. The optimum catalytic performance of TiO_2 depends on a number of parameters which include particle size, surface area, light intensity and the ratio between the anatase and rutile crystal phases present in the actual material [5].

Phenol is an extremely toxic organic compound which is highly soluble in water and a major pollutant. It is used in the manufacture of polymeric resins, herbicides and fungicides it is also used in oil refining, paper mills and in the pharmaceutical industry [6]. Phenol has also become one of the most widely used petrochemical products and demand is increasing and global production of phenol reached 8 million tonnes in 2009 [7]. Since 2001 there has been a 45% increase in demand for the phenol derivative *bisphenol A* for the production of polycarbonate resins used in the manufacture of CDs, CD-ROMs and DVDs [8]. 42% of the global production of phenol is for *bisphenol A* synthesis, followed by phenolic formaldehyde resins at 28% used in the production of circuit boards, coatings and adhesives [9]. Phenol is a protoplasmic poison and poses a major concern to both drinking water and the aquatic environment. It is hazardous to humans as it is corrosive and cellular uptake is rapid after exposure and mainly affects the liver and kidneys but can also affect the respiratory, nervous and cardiovascular systems. Depending on concentration, both short term and long term exposure can cause death [10]. Phenol also inhibits the growth and survival of micro-organisms in biological treatment plants which in turn hinders the degradation of other pollutants [11]. As a result, there are strict guidelines for levels of phenol in drinking and bathing water. The threshold for taste and odour of

* Corresponding author. Tel.: +353 0 21 490 2911/2680.
E-mail address: colmmcman@hotmail.com (C. McManamon).

0304-3894/$ – see front matter © 2011 Elsevier B.V. All rights reserved.
doi:10.1016/j.jhazmat.2011.07.034

phenol has been reported as 150 $\mu g\,l^{-1}$, however, when water is chlorinated in the presence of phenol chlorophenols are formed [12]. These are 2- and 4-chlorophenol, 2,4- and 2,6-dichlorophenol, 2,4,6-trichlorophenol and the taste thresholds are reduced to 0.1, 0.3 and 2 $\mu g\,l^{-1}$, respectively. Due to the risk of chlorophenols at low levels it is recommended by the EU that only 1 $\mu g\,l^{-1}$ of phenol is acceptable in drinking water. The EU has set a guide level of $\leq$5 $\mu g\,l^{-1}$ and a mandatory level of $\leq$50 $\mu g\,l^{-1}$ for bathing waters (Directive 2006/7/EC) [13].

As phenol is an organic compound, photocatalytic decomposition is a popular and economically viable method of degradation [10]. The most common method is the use of a catalyst under a radiation high pressure UV lamp. Chiou and Juang [6] removed 50 $mg\,l^{-1}$ of phenol over 2 h with a 400 W UV lamp using Pr-doped TiO_2. Akbal and Nur Onar [14] used a commercial photocatalyst from Merck Chemical Company and a 300 W UV lamp to remove 99% of phenol, from wastewater, in the presence of H_2O_2. The most popular and worldwide photocatalyst is Evonik's (formally Degussa) P25. This is because of its availability and the fact that it has an almost ideal composition of rutile to anatase (80%:20%) [5]. The photocatalytic properties of P25 on 100 $mg\,l^{-1}$ of phenol degradation were studied by Laoufi et al. [11] using a 15 W and a 400 W UV lamp. It was shown that over 2 h the 15 W lamp removed only 2% of the phenol while the 400 W lamp removed 99%. Photo-oxidation is not the only technique used for phenol removal from wastewater. More recently the use of activated carbon and other catalysts as a support for TiO_2 has also attracted much attention as the support can increase uptake [15]. However, activated carbon is a less effective method, with average results of between 50 and 80% removal over 4 h [16]. Phenol can also removed by adsorption on polymeric resins, membrane-based solvent extraction and pervaporation with hydrophobic membranes [7].

In this paper we report on attempts to produce a more effective photocatalyst for removal of phenol from water by engineering high surface area, a desired anatase to rutile ratio and the use of a dopant to improve photocatalytic properties. ZrO_2 was chosen because it appeared to be the most promising of a series of dopants used in trial results [17].

2. Experimental

2.1. Synthesis of ZrO_2 doped TiO_2

TiO_2 was synthesised according to a modified method by Reidy et al. [18]. Pluronic P123 (3 g) was dissolved in anhydrous ethanol (30 ml), HCl (2.5 ml) and H_2O (0.5 ml) at room temperature. The triblock co-polymer P123 is preferred for its combination of hydrophobic and hydrophilic molecules which form a corona in solution. When the temperature and P123 concentration is increased, the structure moves from cubic to hexagonal ordering as a result of the external hydrophobic character of the co-polymer [19]. Titanium (IV) butoxide (14 ml) was then added with acetylacetone (acac) at a molar ratio of 10:1 (Ti:acac) to adjust the titanium oxide precursor hydrolysis rate. This sol–gel was aged in air for 5 days and was calcined for 6 h at temperatures ranging from 400 to 1000 °C depending on the desired anatase:rutile ratio. Although it is generally accepted that anatase has greater photocatalytic activity than rutile a mixture of both phases is required for efficient photocatalysis.

In situ zirconia doped TiO_2 was prepared with Ti:ZrO_2 molar ratios of 25:1, 50:1, 100:1 and 200:1. These are called Zr 25/1, Zr 50/1, Zr 100/1 and Zr 200/1, respectively. The precursor used for the ZrO_2 doping was zirconium acetylacetonate ($Zr(acac)_4$) and was added at the same time as the titanium (IV) butoxide.

2.2. Characterization methods

Powder X-ray diffraction (PXRD) profiles were recorded on a PANalytical X'Pert diffractometer, equipped with a Cu Kα radiation source and X'Celerator detector. Anatase and rutile percentages were calculated from the resulting diffractograms by using the Spurr equation [20]:

$$\%R = \frac{1}{1 + 0.8[I_A(1\,0\,1)/I_R(1\,1\,0)]} \times 100 \quad (1)$$

where I_A is the intensity of the anatase (1 0 1) peak and I_R is the intensity of the rutile (1 1 0) peak. The surface areas of the calcined TiO_2 catalysts were measured using nitrogen BET isotherms at 77 K on a Micromeritics Gemini 2375 volumetric analyzer. Each sample was degassed for 5 h at 473 K prior to a BET measurement. TEM images were obtained using a FEI TITAN TEM operating at 80–300 kV. Diffuse reflectance infrared Fourier transform spectroscopy (DRIFTS) were recorded on a Bio-Rad FTS 3000 IR Spectrometer.

The Scherrer equation was used to determine rutile crystallite size from the PXRD data:

$$D = \frac{k\lambda}{\beta \cos\theta} \quad (2)$$

where D is the crystallite size, k is a constant, λ is the wavelength of the X-ray radiation, β is the line width (obtained after correction for the instrumental broadening) and θ is the diffraction angle [18].

2.3. Phenol degradation

Phenol concentrations of between 5 and 40 $mg\,l^{-1}$ were prepared using redistilled phenol from 99+% purity chemicals from Sigma–Aldrich. Photocatalytic reactions were carried out under a 40 W UV lamp at 365 nm wavelengths. Analysis was done using UV–vis spectroscopy at a maximum absorption peak of 270 nm. A calibration curve was constructed and degradation results were obtained from the equation given below. Undoped TiO_2 and ZrO_2 doped TiO_2 of metal molar ratios (Ti:Zr) 200:1 (Zr 200/1), 100:1 (Zr 100/1) and 50:1 (Zr 50/1) were tested for phenol degradation. The data for Zr 25/1 was omitted as it displayed extremely poor catalytic results. Dark studies were also tested and showed very little phenol adsorption. Evonik's commercially available P25 was also tested for comparative results. The degradation rate of phenol could be obtained by:

$$D_e = \frac{C_0 - C_t}{C_0} \times 100\% \quad (3)$$

where D_e is the degradation rate of phenol after t min of reaction, C_t is the concentration of phenol after t min of reaction, and C_0 is the initial concentration. The reaction can be explained as follows [1]:

$$TiO_2 + h\nu \rightarrow e^- + h^+ \quad (4)$$

$$e^- + O_2 \rightarrow O_2{}^{-\bullet} \quad (5)$$

$$h^+ + TiO_2 \rightarrow OH^\bullet + h^+ \quad (6)$$

$$\text{Phenol} + OH^\bullet \rightarrow CO_2 + H_2O \quad (7)$$

where $h\nu$ is the light source and e^- represents excited electrons in the conduction band and h^+ represents positive hole pairs in the valance band. This results in the production of free radicals which decompose phenol production CO_2 and H_2O.

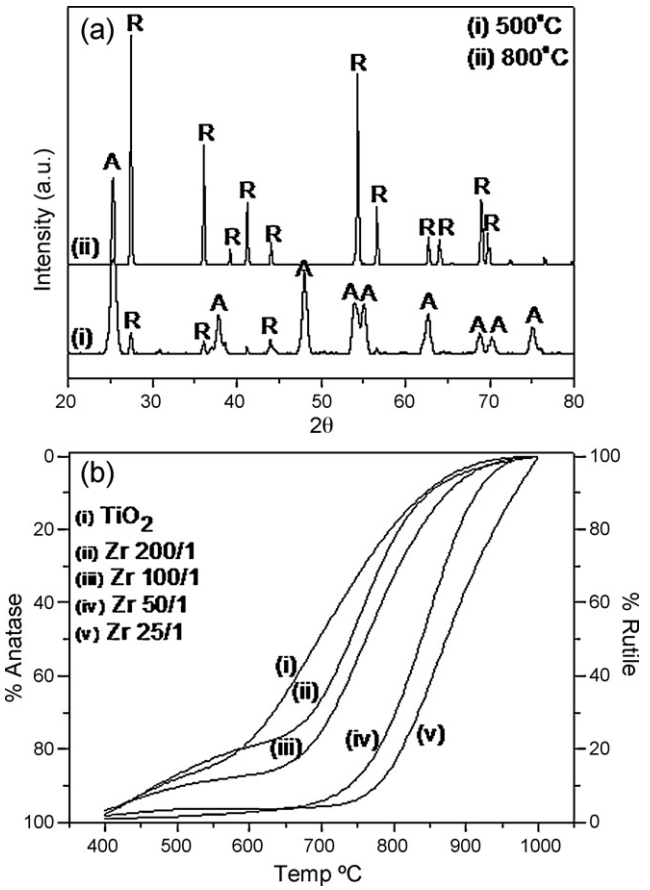

Fig. 1. (a) PXRD of TiO_2 calcined at 500 °C (lower) and 800 °C (upper). Reflection assignment shown: A = anatase and R = rutile. (b) Effect of ZrO_2 loading and temperature on anatase to rutile transformation.

3. Results and discussion

3.1. PXRD

The PXRD data shows only an anatase phase up to 500 °C after which the transformation to the rutile phase begins. Fig. 1(a) shows the two distinct phases at 500 °C and at 800 °C between which there is a rapid conversion in the crystalline polymorph (see Fig. 1(b) for details). This is accompanied by a large decrease in surface area due to a rapid growth of crystallites (Table 1). Table 1 also shows that the incorporation of ZrO_2 "strengthens" the porous TiO_2 structure and reduces the rate of pore collapse as higher surface areas are observed for the ZrO_2 containing samples. There are two possible mechanisms for the anatase to rutile transformation. The undoped TiO_2 particles can agglomerate rapidly at higher temperatures via a grain growth process. With the doped materials, grain growth is inhibited and particle growth occurs due to a "ripening" process where smaller structures are added to the larger grains. In both cases, because of the difference in thermodynamic stability of the two phases at the surface and the bulk, once a critical crystalline size is reached a spontaneous phase change occurs. These mechanisms are described in detail elsewhere [18].

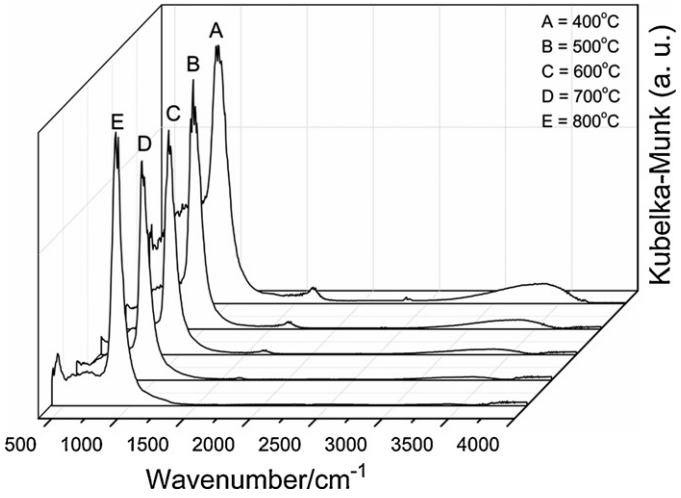

Fig. 2. DRIFTS data for TiO_2 at 400–800 °C.

3.2. DRIFTS

IR data were also consistent with the PXRD data. Fig. 2 shows typical data for the TiO_2 samples calcined at different temperatures. Similar data was observed for all other materials. In all data, a broad peak between 2600 and 3600 cm^{-1} can be seen and this is caused by the stretching vibrations of hydrogen bonded hydroxyl groups and surface water molecules. There is also the presence of some weaker bands at 1700 cm^{-1} due to vibrations from coordinated water as well as from the Ti–OH group. These bands are eradicated upon calcination at higher temperatures as a result of the removal of the hydroxyl groups from the surface of the TiO_2 [21]. Calcination at higher temperatures also displays a peak at 450 cm^{-1} which can be attributed to a Ti–O vibration in the rutile crystalline phase. The large peak at 900 cm^{-1} is a band common to all TiO_2 materials [22].

Table 1
Physiochemical properties of TiO_2 and ZrO_2-doped TiO_2 at selected temperatures of 400 °C, 800 °C and the optimum temperature for ideal anatase:rutile ratio of 80:20 (approx.) (*material used in degradation tests).

Catalyst	Temp. (°C)	% Anatase[a]	% Rutile[a]	Surface area[b] ($m^2\ g^{-1}$)	Rutile crystallite size[a] (nm)
TiO_2	400	98.2	1.8	115	3.5
*	625	79	21	34.6	43.1
	800	16	84	8.3	55.3
TiO_2 (Zr 200/1)	400	98	2	137.3	3.2
*	600	78.3	21.7	49.5	26.5
	800	4.2	95.8	6.5	52.4
TiO_2 (Zr 100/1)	400	96.7	3.3	161.18	2.7
*	700	83.6	16.4	37.2	30.6
	800	27.8	72.2	13.3	43.6
TiO_2 (Zr 50/1)	400	98.3	1.7	140.4	1.8
*	800	81	19	24.7	41.4
	900	2.6	97.4	13.5	45.8

[a] As determined by PXRD.
[b] As determined by nitrogen adsorption (BET method).

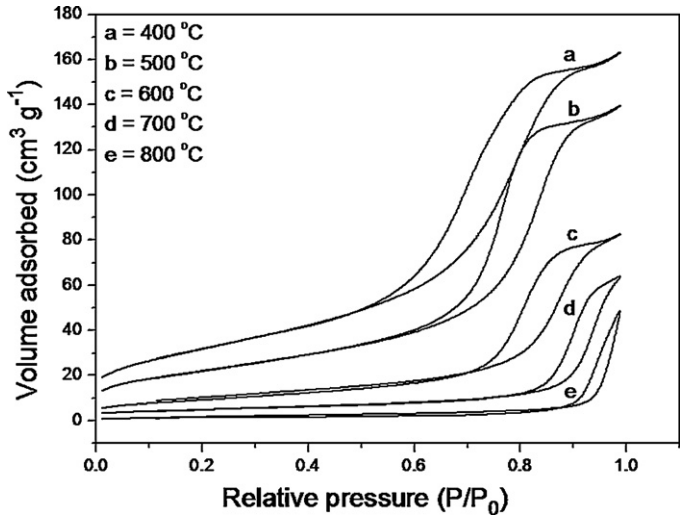

Fig. 3. Typical BET isotherm of TiO_2 as a function of temperature.

3.3. BET

Fig. 3 shows typical BET isotherm data for TiO_2 calcined at 400–800 °C. Other samples showed similar data. According to the IUPAC isotherm classification the graph displays a type V isotherm. This is usually indicative of a mesoporous structure and probably results from a strong affinity between the particles resulting in mesoporous "cavities" amongst the agglomerated nanoparticles. This is supported by TEM imaging in Fig. 4 where the particles are seen to form agglomerates with well-defined free-volumes between them. As the temperature is increased, the free volume is reduced due to sintering mechanisms.

3.4. TEM

A TEM image of TiO_2 calcined at 400 °C (Fig. 4) shows that all particles appear to be less than 10 nm in size and the images are consistent with the formation of inter-particulate pores as described above. Fig. 4(a) shows a high degree of agglomeration present. Closer imaging shows some uniform angstrom sized structures of the nanoparticles (Fig. 4(b)). This appears to be an image of a small crystallite where lattice spacing can be clearly seen. However, in Fig. 4(c) the structure seems to show an unusual "track" structure. This may be due to the presence of P123 which provides a form of molecular templating and results in micropore channels.

3.5. Effect of pH on degradation of phenol

Materials were calcined to provide an optimum anatase:rutile content and were used for phenol degradation (see Table 1 for details). The pH of the solution in which phenol is dissolved has a major role in the photocatalytic degradation of phenol as the surface charge state of TiO_2, the flat-band potential and the dissociation of phenol are all pH dependant [23]. Industrial wastes, unlike municipal wastewater, may be basic or acidic and, as this is the source of most environmental phenols, it is an important parameter to be considered. The flat-band potential is an essential part of any semiconductor electrolyte system on which the band gap energy of the valance band and conduction band are dependent [24]. The isoelectric point (IEP) is the pH at which the surface of a material has no charge due to an equal amount of positive and negative charges. Fig. 5 shows the IEP of TiO_2 and ZrO_2-doped TiO_2 to be at pH 6.2. There is no change in the pH of the doped materials as the level of doping does not affect the surface charge of the catalyst. A positive surface charge is predicted at a pH below this point while a negatively charged surface is expected under more alkaline conditions [25]. Under acidic conditions phenol is primarily nega-

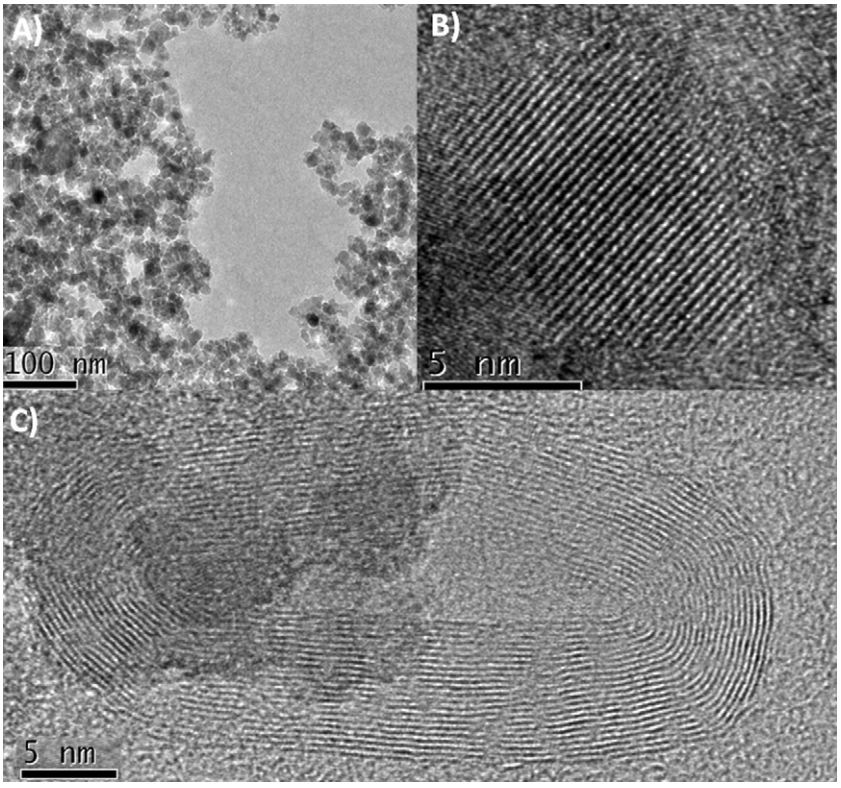

Fig. 4. TEM of undoped TiO_2 calcined at 400 °C: (a) agglomeration of TiO_2 particles, (b) small crystallite displaying lattice spacing and (c) shows a "track" structure.

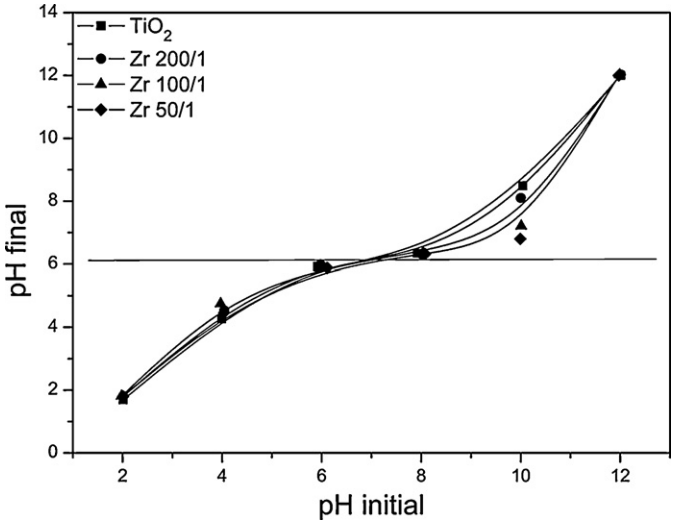

Fig. 5. IEP of ZrO_2-doped and undoped TiO_2.

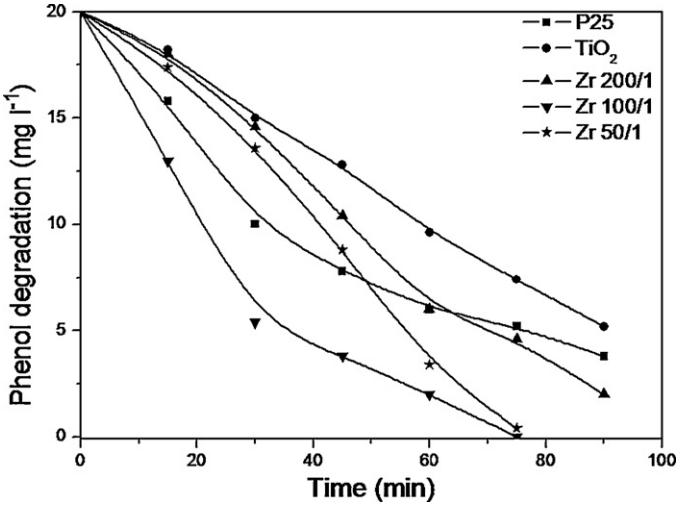

Fig. 7. Degradation of phenol using ZrO_2 doped and undoped TiO_2 over time at pH 5.

tively charged and this allows for easier adsorption to the surface of the positively charged TiO_2. Additionally, at a more acidic pH phenol is not dissociated and this allows for a maximum number of phenol molecules adsorbed onto the TiO_2 surface [26].

Typical data of the decomposition of phenol (20 mg l^{-1}) at varying pH levels is shown in Fig. 6. ZrO_2 doped materials display the highest rates of degradation when compared to the undoped TiO_2 and P25. Degradation below pH 3 and above pH 7 does not favour the oxidation of phenol with pH 5 displaying the best results. It is suggested that at pH levels below 3 the TiO_2 surface is covered in H^+ ions which reduces the formation of OH radicals. Between pH 3 and 7 the surface of the TiO_2 is less able to hold protons, the release of these protons causes a reaction with hydroxyl ions and produces more radical hydroxide but can also alter the pH of solution by up to 3 units [27]. At higher pH levels the formation of hydroxyl radicals is reduced due to competition from phenoxide species for adsorption sites [11]. Thus, about pH 5 is the optimum value for the rapid generation of OH radicals as well as their unhindered regeneration in the absence of either phenoxide ions or H^+ ions. This gives the TiO_2 a positive charge which attracts the negatively charged phenol onto the surface of the catalyst resulting in efficient degradation. At a higher pH, the loss of H^+ ions from the hydroxyl group of ions forms a negative phenolate ion which repels the negatively charged TiO_2. This is consistent with many studies in literature, Bekkouche et al. [28] found optimum decomposition just below the isoelectric point at pH 5–6. The isoelectric point (IEP) is the pH at which the surface of a material has no charge due to an equal amount of positive and negative charges. Kashif and Ouyang [29] also observed highest degradation efficiency at pH 5 corresponding to a pH_{pzc} of 6.8. The authors go on to suggest that carbonate ions are the limiting factor at high pH as they act as scavangers for OH^- ions.

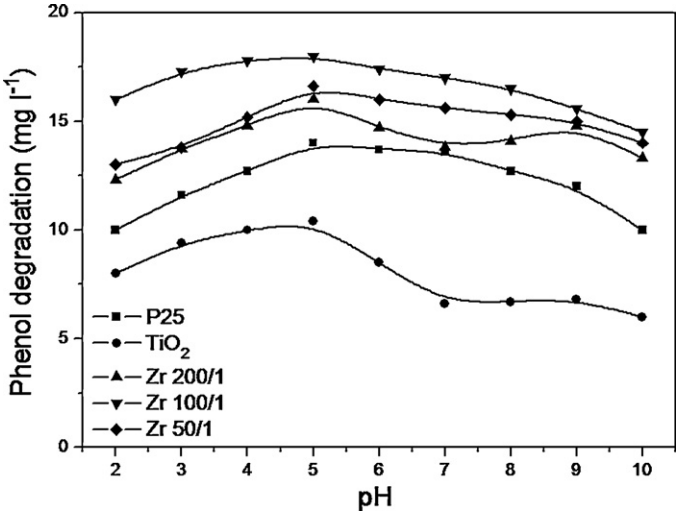

Fig. 6. Effect of pH on phenol degradation (20 mg l^{-1}) using 0.5 wt% of catalyst over a period of 60 min.

Further analysis of the degradation of phenol with time at pH 5 again shows that Zr 100/1 obtains the best results by decomposing 20 mg l^{-1} of phenol in 75 min (Fig. 7). The next highest sample was Zr 50/1 followed by Zr 200/1 all of which were considerably better than the P25 which only achieved 75% degradation after 75 min. The undoped TiO_2 sample also performed poorly indicating that the incorporation of zirconia is crucial in achieving high rates of degradation. It is suggested that photocatalytic enhancement cannot be attributed to the ability of ZrO_2 to hinder the aggregation of the TiO_2 particles and increasing the number of surface active sites [30]. Instead, it is proposed that the replacement of Ti lattice ions with Zr ions creates a space charge region creating an electric force which improves the separation efficiency of the electron–hole pairs [2]. This also acts as an electron trap slowing down the rate of recombination lengthening the lifetime of the hydroxyl radicals. As there are two types of recombination (a) surface recombination and (b) volume recombination both mechanisms require consideration. Doping reduces surface recombination whereas volume recombination can only be reduced by particle size synthesis. However, excess doping reduces the mobility of the charge carriers which increases the surface recombination rate resulting in a shortened life span of the hydroxyl radicals [31].

3.6. Effect of phenol concentration on photocatalytic decomposition

The effect of phenol concentration on degradation, at equilibrium time (75 min), is represented in Fig. 8. Concentrations were tested between 5 and 40 mg l^{-1} using 0.5 wt% of catalyst. The initial increase of concentration gives a significant increase of decomposition using the same amount of TiO_2. Degradation of phenol peaks at 25 mg l^{-1} meaning that this is the maximum level for efficiency. As the concentration of phenol is increased, using the same mass of TiO_2, there is a greater number of phenol molecules. These attach to the surface active sites occupying them to capacity forming a "pas-

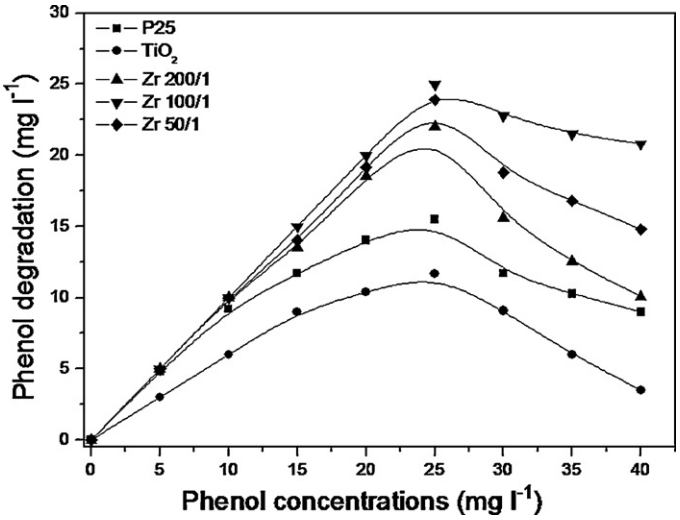

Fig. 8. Effect of phenol concentration on phenol degradation (see text for details).

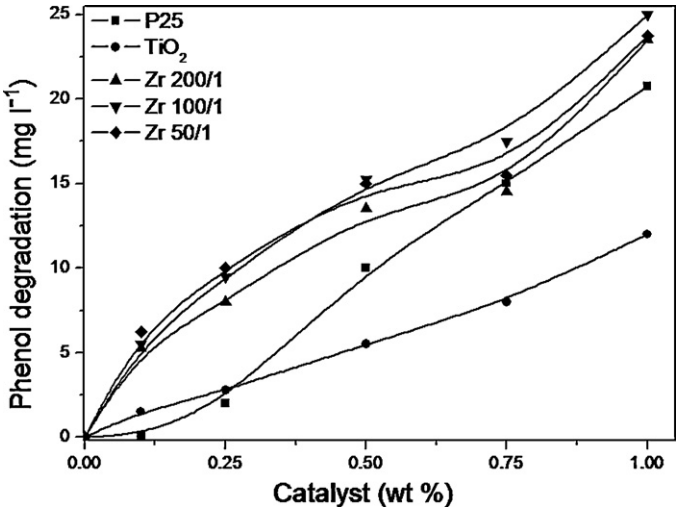

Fig. 9. Effect of catalyst loading on degradation of phenol at equilibrium time.

sivating" monolayer [28]. This inhibits additional phenol molecules being adsorbed onto the TiO_2 surface, hence, the reduction in photocatalytic degradation.

The maximum amount of phenol decomposed per gram per hour per watt is displayed in Table 2. The values compare well to other studies in this area. Chiou and Juang [6] decomposed phenol at a rate of 0.1075 mg g^{-1} h^{-1} W^{-1} using Pr-doped TiO_2 under a much higher light intensity at 400 W. Similarly, Mu et al. [32] degraded 0.112 mg g^{-1} h^{-1} W^{-1} of phenol from solution using a 125 W high pressure mercury lamp. While Zhang and Gao [5] used undoped TiO_2 nanoparticles to decompose phenol at a rate of 0.075 mg g^{-1} h^{-1} W^{-1}. This suggests that the ZrO_2-doped samples achieve a very high level of phenol degradation under a 40 W lamp and better results are likely at exposure to greater light intensity.

3.7. Effect of catalyst loading on degradation of phenol

The catalyst loading for ZrO_2-doped TiO_2 was varied from 0.1 to 1 wt% using a 25 mg l^{-1} phenol solution to find optimum loading and avoid an ineffective excess of catalyst within the system. It was observed that the maximum degradation, unsurprisingly, was obtained as the quantity of catalyst increased. However, 0.5 wt% appears to be about the most efficient at decomposing phenol with the ZrO_2-doped samples. Zr 200/1, Zr 100/1 and Zr 50/1 decompose 54%, 61% and 62%, respectively, in 60 min and only an extra 40%, 39% and 33% decomposition is achieved by doubling the quantity of the catalyst. The possible explanation for this is that increased catalyst loading generates more electron–hole pairs forming $OH^{\bullet}$ radicals leading to the enhancement of photocatalysis. In spite of this, decomposition is not doubled due to the excess of catalyst decreasing the light penetration through the solution and so reducing the maximum efficacy of the TiO_2. Particles also tend to agglomerate under these conditions reducing the accessibility of both phenol molecules and radiation to the surface active sites of the catalyst [33] (Fig. 9).

Table 2
Maximum degradation of phenol (mg g^{-1} h^{-1} W^{-1}).

Catalyst	Degradation rate
P25	0.155
TiO_2	0.117
TiO_2 Zr 200/1	0.210
TiO_2 Zr 100/1	0.249
TiO_2 Zr 50/1	0.229

3.8. Kinetics

The Langmuir–Hinshelwood kinetic model was initially developed to quantitatively describe gaseous–solid reactions and is now the most commonly used method of expressing the heterogeneous catalytic process [34]:

$$r = -\frac{dc}{dt} = \frac{k_r K c}{1 + Kc} \tag{8}$$

where r is the rate of reaction that changes with time (mg l^{-1} min^{-1}), K is the equilibrium constant for adsorption of the substrate onto catalyst, C is the concentration at any time during degradation (mg l^{-1}), k_r is the limiting rate constant of reaction at maximum coverage under the given experimental conditions and t is the time. This can be simplified to a first-order reaction and expressed as follows:

$$\ln \frac{C_0}{C} = k_{(app)} \times t \tag{9}$$

where C_0 is the initial concentration of the pollutant, C is the concentration at any time during degradation (mg l^{-1}) and t is the irradiation time. By plotting $\ln(C_0/C)$ versus t (time), the apparent rate constant $k_{(app)}$ can be determined from the slope of the curve obtained. This then means the kinetic of phenol degradation is of pseudo first-order, at $t = 0$ and $C = C_0$ becomes:

$$r_0 = \frac{k_r K C_0}{1 + KC_0} \tag{10}$$

This equation can then be rearranged into linear form:

$$\frac{1}{r_0} = \frac{1/k_r K}{1/C_0 + 1/k_r} \tag{11}$$

where $1/r_0$ is the dependent variable, $1/C_0$ is the independent variable, $1/k_r$ is the linear coefficient and $1/k_r K$ is the angular coefficient of the straight line. From this model, the Langmuir–Hinshelwood adsorption constant and the rate constant were obtained by plotting $1/r_0$ versus $1/C_0$ (Fig. 10) [11].

The representation of $1/r_0$ versus $1/C_0$, as shown in Fig. 10 in the presence of different concentrations of phenol at time versus initial phenol concentration yields a straight line indicating a pseudo first-order reaction. The reaction rate constants for photocatalytic degradation of phenol were evaluated from experimental data using a linear regression. For all the materials the R^2 (correlation coefficient) value was higher than 0.999 which confirms the proposed kinetics for degradation of phenol in this process (Table 3).

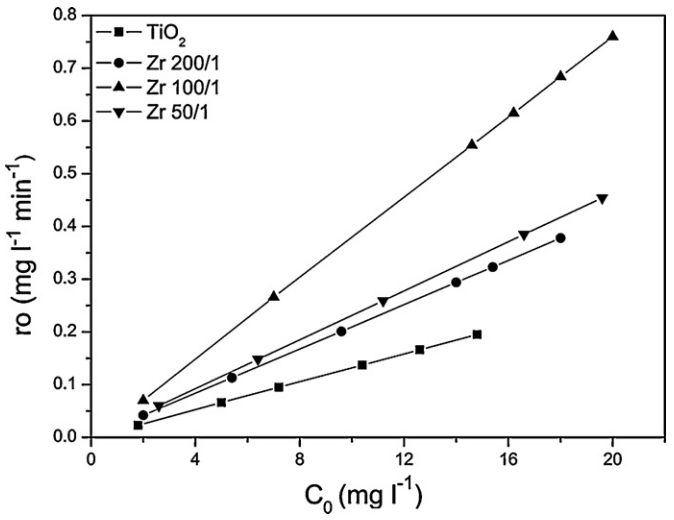

Fig. 10. Plotted data using linearization of Langmuir–Hinshelwood's equation.

Table 3
First-order rate constants $k_{(app)}$ and linear regression coefficients.

Material	$k_{(app)}$ ($\ln(C_0/C)$ versus t)	R^2
TiO_2	0.016	0.999
Zr 200/1	0.028	0.999
Zr 100/1	0.039	0.999
Zr 50/1	0.035	1

3.9. Reuse of TiO_2

An important factor on the economic viability of this material is its ability to be reused. The reuse of the best sample (Zr 100/1) was tested and shown in Fig. 11. There is an expected decrease in photocatalytic activity from 25 mg l^{-1} removed after 75 min to 22.1 mg l^{-1} removed after 75 min upon 5th use. The decrease in activity could be assigned to either loss of surface area or due to deposition of reaction products at the catalyst surface. However, changes in activity are small and the reused catalyst will decompose 100% of the 25 mg l^{-1} over a slightly longer period of time. The 2.3% reduction upon each use of the material is a result of a loss in surface active sites. This is mainly due to poisoning of the catalyst by reaction by-products formed in the pollutant breakdown which are adsorbed onto the surface of the catalyst Another reason is the impossibility of restoring the initial dispersity of the particles of the catalyst on repeated use [35]. These results compare favourably to previous studies [14,36].

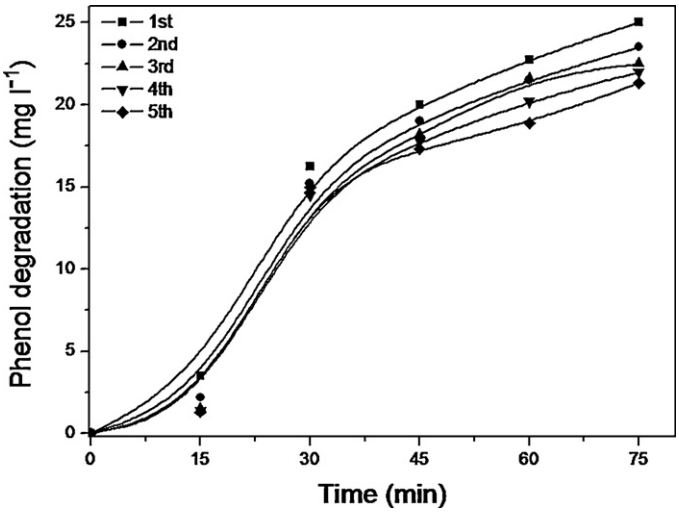

Fig. 11. Reuse of Zr 100/1.

4. Conclusions

Presented in this paper is a simple method of synthesising anatase (>99%) titanium dioxide nanoparticles. Calcination of the powders at temperatures above 500 °C resulted in the transformation to the rutile phase of TiO_2. The incorporation of zirconia helped stabilize the anatase phase up to higher degrees. This allowed for an ideal anatase to rutile ratio and larger surface area. TEM images showed sub 10 nm relatively uniform particles. The most promising samples were used to decompose phenol, an extremely toxic chemical, under UV radiation. TiO_2 doped with 1% (molar metal content) of zirconia (Zr 100/1) at pH 5 proved to be the best catalyst removing 0.0249 mg g^{-1} h^{-1} W^{-1}. This compares extremely well to the 0.155 mg g^{-1} h^{-1} W^{-1} achieved by Evonik's commercial catalyst P25. It was determined that the optimum amount of ZrO_2-doping has number of advantages over undoped TiO_2 but excess dopant reduces the efficiency of the catalyst. Optimum doping allowed for a quicker separation of electron–hole pair and this also resulted in slower recombination. The Langmuir–Hinshelwood kinetic model was applied to degradation data, from all synthesised catalysts, to obtain the rate of reaction. The R^2 correlation coefficient values were higher than 0.999 showing a good fit. The reuse of the catalyst Zr 100/1 was also tested and was found to achieve very high decomposition rates after repeated use.

Acknowledgments

We acknowledge financial support from the EPA STRIVE scheme (Grant Code 2009-PhD-ET-15). We also thank Sozaraj Rasappa for his help with TEM imaging. This research is independent of the Irish Environmental Protection Agency and does not necessarily reflect the views of the agency and no official approval should be assumed.

References

[1] A. Fujishima, K. Honda, Electrochemical photolysis of water at a semiconductor electrode, Nature 238 (1972) 37–38.
[2] K. Hashimoto, I. Hiroshi, A. Fujishima, TiO_2 photocatalysis: a historical overview and future prospects, Japanese Journal of Applied Physics 44 (2005) 8269–8285.
[3] S.N. Frank, A.J. Bard, Heterogeneous photocatalytic oxidation of cyanide ion in aqueous solutions at titanium dioxide powder, Journal of the American Chemical Society 99 (1977) 303–304.
[4] S. Guo, Z.B. Wu, W.R. Zhao, TiO_2-based building materials: above and beyond traditional applications, Chinese Science Bulletin 54 (2009) 1137–1142.
[5] Q. Zhang, L. Gao, Preparation of nanocrystalline TiO_2 powders for photocatalytic oxidation of phenol, Research on Chemical Intermediates 35 (2009) 281–286.
[6] C.-H. Chiou, R.-S. Juang, Photocatalytic degradation of phenol in aqueous solutions by Pr-doped TiO_2 nanoparticles, Journal of Hazardous Materials 149 (2007) 1–7.
[7] W. Kujawski, A. Warszawsk, W. Ratajczak, T. Porebski, W. Capata, I. Ostrowska, Removal of phenol from wastewater by different separation techniques, Desalination 163 (2004) 287–296.
[8] M.F. Fernandez, J.P. Arrebola, J. Taoufiki, A. Navalon, O. Ballesteros, R. Pulgar, J.L. Vilchez, N. Olea, Bisphenol-A and chlorinated derivatives in adipose tissue of women, Reproductive Toxicology 24 (2007) 259–264.
[9] SRIconsulting World Petrochemical Report: Phenol 2010 http://www.sriconsulting.com/WP/Public/Reports/phenol/.
[10] D. Fabbri, A. Bianco Prevot, E. Pramauro, Effect of surfactant microstructures on photocatalytic degradation of phenol and chlorophenols, Applied Catalysis B 62 (2006) 21–27.
[11] N.A. Laoufi, D. Tassalit, F. Bentahar, The degradation of phenol in water solution by TiO_2 photocatalysis in a helical reactor, Global NEST Journal 10 (2008) 404–418.
[12] J.A. Field, R. Sierra-Alvarez, Microbial degradation of chlorinated phenols, Reviews in Environmental Science and Biotechnology 7 (2008) 211–241.
[13] EPA, http://www.bathingwater.ie/epa/background.htm.
[14] F. Akbal, A. Nur Onar, Photocatalytic degradation of phenol, Environmental Monitoring and Assessment 83 (2003) 295–302.

[15] J. Matos, J. Laine, J.-M. Herrmann, Effect of the type of activated carbons on the photocatalytic degradation of aqueous organic pollutants by UV-irradiated titania, Journal of Catalysis 200 (2001) 10–20.
[16] E. Carpio, P. Zuniga, S. Ponce, J. Solis, J. Rodriguez, W. Estrada, Photocatalytic degradation of phenol using TiO_2 nanocrystals supported on activated carbon, Journal of Molecular Catalysis A 228 (2005) 293–298.
[17] C. McManamon, Development of Chemically Engineered Nanoporous Materials for Water Pollution Remediation, University College Cork, Cork, 2011.
[18] D.J. Reidy, J.D. Holmes, M.A. Morris, Preparation of a highly thermally stable titania anatase phase by addition of mixed zirconia and silica dopants, Ceramics International 32 (2006) 235–239.
[19] S.L. Yuan, X.Q. Zhang, K.Y. Chan, Effects of shear and charge on the microphase formation of P123 polymer in the SBA-15 synthesis investigated by mesoscale simulations, Langmuir 25 (2009) 2034–2045.
[20] W. Nuansing, S. Ninmuang, W. Jarernboon, S. Maensiri, S. Seraphin, Structural characterization and morphology of electrospun TiO_2 nanofibers, Materials Science and Engineering B: Solid State Materials for Advanced Technology 131 (2006) 147–155.
[21] D.L. Pavia, G.L. Lampman, G.S. Kriz, J.R. Vyvyan, Introduction to Spectroscopy, 4th ed., Brooks/Cole, 2009, p. 744.
[22] C.G. Silva, J.L. Faria, Anatase vs. rutile efficiency on the photocatalytic degradation of clofibric acid under near UV to visible irradiation, Photochemical & Photobiological Sciences 8 (2009) 705–711.
[23] T.-T. Wei, C.-C. Wan, Heterogeneous photocatalytic oxidation of phenol with titanium dioxide powders, Industrial & Engineering Chemistry Research 30 (1991) 1293–1300.
[24] K. Gelderman, L. Lee, S.W. Donne, Flat-band potential of a semiconductor: using the Mott–Schottky equation, Journal of Chemical Education 84 (2007) 685–688.
[25] S.P. Devipriya, S. Yesodharan, Photocatalytic degradation of phenol in water using TiO_2 and ZnO, Journal of Environmental Biology 31 (2010) 247–249.
[26] S.K. Pardeshi, A.B. Patil, A simple route for photocatalytic degradation of phenol in aqueous zinc oxide suspension using solar energy, Solar Energy 82 (2008) 700–705.
[27] N. Ngadi, S.K. Jamaludin, Effects of pH on ethanol photocatalytic oxidation using TiO_2 and zeolite 13X as catalyst, Jurnal Teknologi 43 (2007) 27–38.
[28] S. Bekkouche, M. Bouhelassa, N.H. Salah, F.Z. Meghlaoui, Study of adsorption of phenol on titanium oxide (TiO_2), Desalination 166 (2004) 355–362.
[29] N. Kashif, F. Ouyang, Parameters effect on heterogeneous photocatalysed degradation of phenol in aqueous dispersion of TiO_2, Journal of Environmental Sciences-China 21 (2009) 527–533.
[30] H.L. Xia, H.S. Zhuang, D.C. Xiao, T. Zhang, Photocatalytic activity of lanthanum and sulfur co-doped TiO_2 photocatalyst under visible light, Journal of Wuhan University of Technology-Materials Science Edition 23 (2008) 467–471.
[31] X.Q. Chen, J.Y. Yang, J.S. Zhang, Preparation and photocatalytic properties of Fe-doped TiO_2 nanoparticles, Journal of Central South University of Technology 11 (2004) 161–165.
[32] R.X. Mu, Z.Y. Xu, L.Y. Li, Y. Shao, H.Q. Wan, S.R. Zheng, On the photocatalytic properties of elongated TiO_2 nanoparticles for phenol degradation and Cr(VI) reduction, Journal of Hazardous Materials 176 (2010) 495–502.
[33] S.J. Royaee, M. Sohrabi, Application of photo-impinging streams reactor in degradation of phenol in aqueous phase, Desalination 253 (2010) 57–61.
[34] K.V. Kumar, K. Porkodi, F. Rocha, Langmuir–Hinshelwood kinetics—a theoretical study, Catalysis Communications 9 (2008) 82–84.
[35] A.G. Zhigotskii, E.F. Rynda, N.A. Mishchuk, V.M. Kochkodan, A.V. Ragulya, V.P. Klimenko, M.N. Zagornyi, A study of the photocatalytic activity of titanium dioxide nanopowders, Russian Journal of Applied Chemistry 81 (2008) 2056–2061.
[36] M.Z. Kassaee, H. Masrouri, F. Movahedi, R. Mohammadi, TiO_2 as a reusable catalyst for the one-pot synthesis of 3,4-dihydropyrimidin-2 (1H)-ones under solvent-free conditions, Helvetica Chimica Acta 93 (2010) 261–264.